Evolution of Length-Dependent Properties of Discrete n-Type Oligomers Prepared via Scalable Direct Arylation

Rukiya Matsidik, Hartmut Komber, Martin Brinkmann, Karl Sebastian Schellhammer, Frank Ortmann, Michael Sommer

Evolution of Length-Dependent Properties of Discrete n-Type Oligomers Prepared via Scalable Direct Arylation

Rukiya Matsidik[a,b], Hartmut Komber[c], Martin Brinkmann[d], Karl Sebastian Schellhammer[e], Frank Ortmann[f], , Michael Sommer[a,b*]

[a] Institut für Chemie, TU Chemnitz, Professur Polymerchemie, Straße der Nationen 62, 09111 Chemnitz, Germany

[b] Forschungszentrum MAIN, TU Chemnitz, Rosenbergstraße 6, 09126 Chemnitz, Germany

[c] Leibniz-Institut für Polymerforschung Dresden e.V., Hohe Straße 6, 01069 Dresden, Germany

[d] Université de Strasbourg, CNRS, ICS UPR 22, F-67000 Strasbourg, France

[e] Dresden Integrated Center for Applied Physics and Photonic Materials (IAPP) and Institute for Applied Physics, TU Dresden, Nöthnitzer Strasse 61, 01187 Dresden, Germany

[f] Department of Chemistry, TU München, 85748 Garching b. München, Germany

KEYWORDS n-type oligomers, CH activation, naphthalene diimide, structure function relationships, crystallinity.

ABSTRACT: Efficient organic electronic devices are fabricated from both small molecules and disperse polymers, but materials with characteristics in between remain largely unexplored. Here we present a gram scale synthesis for a series of discrete n-type oligomers comprising alternating naphthalene diimide (NDI) and bithiophene (T2). Using C-H activation, discrete oligomers of type T2-(NDI-T2)$_n$ ($n \leq 7$) and persistence lengths up to ~ 10 nm are made. The absence of protection/deprotection reactions and the mechanistic nature of Pd-catalyzed C-H activation allows to produce symmetrically terminated species almost exclusively, which is key to fast preparation, high yields and the general success of the reaction pathway. The reaction scope includes different thiophene-based monomers, end capping to yield NDI-(T2-NDI)$_n$ ($n \leq 8$) and branching at T2 units by non-selective C-H activation under certain conditions. We show how the optical, electronic, thermal, and structural properties depend on oligomer length along with a comparison to the disperse, polymeric analog PNDIT2. From theory and experiment we find that molecular energy levels are not affected by chain length resulting from the strong donor-acceptor system. Absorption maxima saturate for n = 4 in vacuum and for n = 8 in solution. Linear oligomers T2-(NDI-T2)$_n$ are highly crystalline with large melting enthalpies up to 33 J/g, NDI-terminated oligomers show reduced crystallinity, stronger supercooling and more phase transitions. Branched oligomers and those with bulky thiophene comonomers are amorphous. Large oligomers exhibit similar packing characteristics compared to PNDIT2, making these oligomers ideal models to study length-structure-function relationships at constant energy levels.

Introduction

Molecular weight (MW) and dispersity of conjugated polymers are critical parameters that govern their opto-electric properties to a large extent.[1,2] Both, discrete small molecules and disperse polymeric materials are used in efficient organic electronic devices, such as organic field-effect transistors (OFETs) and photovoltaics (OPVs). For instance, power conversion efficiencies exceeding 10% are now commonly reported for all-polymer OPVs[3–7], while blends of conjugated donor polymers with small molecule acceptors yield yet higher efficiencies in excess of 18%.[8–10] Considering often reported strong molecular weight effects seen with disperse conjugated polymers[1,2,11–15], the influence of chain length on properties is omnipresent but commonly not investigated systematically. The influence of dispersity of a conjugated polymer on properties has been investigated to yet smaller extent.[2,16] This is problematic in the context of exploring the full potential of a new disperse material that is additionally susceptible to batch-to-batch variations (BBV).[2,17,18]

Finding answers is mostly limited by synthetic accessibility of well-defined conjugated systems, that, at the same time, are relevant to efficient devices and can be made at sufficiently large scale. Previous research on the synthesis and properties of discrete oligomers includes phenylenes[19–24], 3-hexylthiophene (3HT) and its derivatives[16,25–28], and more recently diketopyrrolopyrrole-based structures.[29,30] In most cases, synthetic approaches rely on iterative reactions including functionalization for cross-coupling and protection/deprotection strategies, which render

preparation cumbersome and lengthy. Moreover, most studies available report p-type oligomers, while n-type oligomers are scarcely investigated.[31]

Among n-type polymers, the alternating copolymer poly{[N,N′-bis(2-octyldodecyl)-naphthalene-1,4,5,8-bis(dicarboximide)-2,6-diyl]-alt-5,5′-(2,2′-bithiophene)} comprising naphthalene diimide (NDI) and bithiophene (T2) units, here referred to as PNDIT2, is an often used and well-known benchmark n-type polymer. Due to its high electron mobilities, low energetic disorder, and unconventional morphological behavior, PNDIT2 has been the objective of an extensive number of studies and became a staple and representative n-type material.[32–34] Properties of PNDIT2 on the other hand can be largely modulated and enhanced by replacing T2 with other donor units, changing the nature of the side chain on the NDI unit, and/or core extension of the NDI skeleton.[34–38] Consequently, NDI copolymers have been popular targets for a variety of applications such as OFETs, OPVs, organic thermoelectric generators (OTEG), bioelectronics and sensors. [32–34,39,40] Strikingly, unlike classical semiconducting polymers such as P3HT where optoelectrical properties generally improve with increasing MW[41], the FET mobility of PNDIT2-based transistors has been found to be much less dependent on chain length.[12,32,42] To further understand this unconventional MW dependence of PNDIT2, synthesis of well-defined discrete NDIT2 oligomers with varying chain length are of great importance.

Here, we present an optimized and scalable route to prepare discrete n-type oligomers based on naphthalene diimide (**NDI**) and bithiophene (**T2**) up to the octamer via phosphine-free Pd-catalyzed direct arylation (DA). The reaction sequence involves 1-3 steps only depending on length and end group, and does not require the introduction of functional groups or protection/ deprotection steps. The synthetic strategy relies on the preparation of symmetrically T2-terminated NDI oligomers **T2-(NDI-T2)$_n$** with n ≤ 7 by combining DA oligomerization and sequential DA (**Scheme 1a**). The success of this reaction is enabled by i) Pd(0) ring-walking over the NDI skeleton leading to all-T2-termination, ii) an excess of T2 and iii) detailed optimization of reaction parameters. T2-terminated oligomers can be coupled with mono-bromo NDI (**NDIBr**) in quantitative yield under optimized conditions, furnishing defect-free **NDI-(T2-NDI)$_n$** oligomers with n ≤ 8 (**Scheme 1b**). When using increased amounts of **NDIBr** here, non-selective branching at β- and γ-C-H positions of **T2** is observed (**Scheme 1c**). To widen substrate scope, hexylphenyl-substituted indacenodithiophene (**IDT**) instead of T2 is also used (**Scheme 1d**). We finally investigate the molecular, optical, electronic, thermal and structural properties in detail and show how these evolve with oligomer length. Light absorption, effective conjugation length (ECL), and aggregation in solution enhances with chain length and saturates for the largest oligomers, resembling PNDIT2. The largest difference to PNDIT2[32] is their highly crystalline nature. This strategy allows to establish discrete n-type oligomers and thus structure-property relationships to bridge the knowledge gap between small molecules and disperse conjugated polymers for organic electronic applications.

Scheme 1. Synthetic approaches to n-type oligomer preparation. a) Synthesis of symmetrically terminated T2-(NDI-T2)$_n$ oligomers, b) synthesis of symmetrically terminated NDI-(T2-NDI)$_n$ oligomers, c) branching at T2 units by β/γ-arylation and d) thiophene comonomer variation.

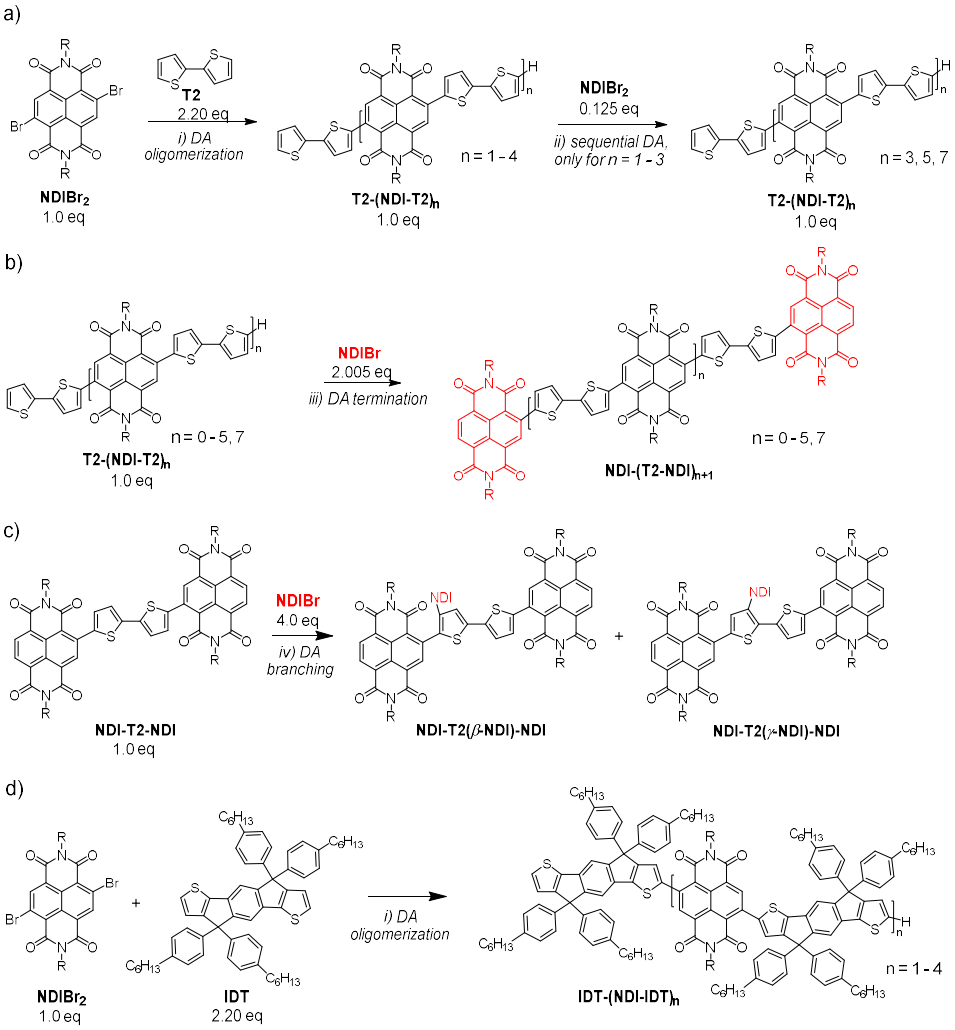

R: 2-octyldodecyl; i) DA oligomerization: Pd_2dba_3 (1 mol.-%), K_2CO_3 (3.0 eq), PivOH (1.0 eq), mesitylene (0.1 M), 90°C, 24 h; ii) sequential DA: Pd_2dba_3 (1 mol.-% for T2, 2 mol.-% for IDT), K_2CO_3 (3.0 eq), PivOH (1.0 eq), mesitylene (0.1 M), 90°C; iii) DA termination: Pd_2dba_3 (3 mol.-%), K_2CO_3 (3.0 eq), neodecanoic acid (1. 0 eq), mesitylene (0.1 M), 80 °C, 48 h; iv) DA branching: Pd_2dba_3 (3 mol.-%), Na_2CO_3 (3.0 eq), PivOH (1.0 eq), 120 °C, 72h.

Results and Discussion

Oligomer synthesis and termination

During previous kinetic studies of PNDIT2 synthesis via direct arylation polymerization (DAP), we hypothesized that the second oxidative addition of Pd(0) into the second C-Br bond of $NDIBr_2$ must proceed in an intramolecular fashion, and therefore is expected to be much faster than the first one.[43] The underlying mechanistic feature of this phenomenon, observed also for the synthesis of PNDIT2 via Stille polycondensation[44], presumably originates from a π-complex between a Pd(0)L species (L= ligand) and the NDI skeleton, over which Pd(0)L "ring walks" to undergo fast oxidative addition into the second NDI-Br bond.[45] Although we did not observe such π-complex directly, we assume its presence on the basis of the observed prevalent T2-termination.[43] We also note that such ring walking processes are well-known from Ni-catalyzed cross couplings, where Ni(0)-NDI complexes have been directly proven.[46–48] As a consequence of the faster intramolecular second oxidative addition, exclusive T2-termination of prepolymers occurs in the beginning of the reaction. At later stages of polycondensation, these react with remaining $NDIBr_2$ monomer to give chains of much higher MW. Such mechanism greatly facilitates preparation and isolation of T2-terminated species which form at high yield and at early stages of polycondensation. Therefore, we first attempted to prepare symmetrically T2-teminated NDI oligomers via time-controlled DAP under standard DAP conditions,[42,49] in which an excess of T2 controls chain length and additionally favors all-T2 termination.[42] Upon monitoring the process with thin layer chromatography (TLC), the number of product TLC spots increases from one at early stages to up to 5 within 2h (**Scheme S1**). To avoid formation of high MW species that decrease the yield of oligomers and also impede separation, the reaction was terminated after 5h. Oligomers **T2-(NDI-T2)$_n$** with **n = 1-4** were isolated in yields between 20-3 % (for details see Supporting Information and **Table S1**). However, detailed analysis by ^{1}H NMR spectroscopy and MALDI-ToF mass spectrometry (MALDI-ToF MS) showed

the presence of small amounts of asymmetrically **T2/NDIBr**-terminated species. While **T2-NDIBr** can be isolated, larger asymmetrically terminated species could not be removed chromatographically. For instance, ^{1}H NMR analysis indicated an end group ratio **T2/NDIBr** = 77:23 for seemingly isolated **T2-(NDI-T2)$_4$**. Thus, while the ring walking mechanism clearly contributes to the dominance of T2 termination, it alone does not readily cause their exclusive presence. A further challenge encountered with time-controlled DAP is associated with large batch-to-batch variation (BBV). For example, changing the batch size of an optimized reaction did not lead to reproducible results.

Therefore, aiming to eliminate both **NDIBr** termination and BBV, the reaction of **NDIBr$_2$** with a much larger excess of T2 and K_2CO_3 as base was targeted, here referred to as "DA oligomerization" (**Scheme 1a**, conditions i), see additional results compiled in **Figure S1**). Depending on the feed ratio **NDIBr$_2$:T2**, the number of different oligomers and their yield can be tuned (**Table S2**). A ratio of 1: 2.2 produces symmetrically terminated **T2-(NDI-T2)$_n$** oligomers (**n = 1-4**) in good yields. For this off-stoichiometry experiment, a comparison of the expected and experimentally found number average degree of polymerization DP_n is carried out. The experimental DP is smaller than what is expected from the Carother´s equation, which is a result of the ring walking process (see additional results compiled in **Figure S2**). A ratio of 1:10 furnishes **T2-(NDI-T2)$_1$** in 92 % yield (**Table 1**). From this result it appears logic to produce larger oligomers with n> 1 by adjusting the feed ratio. However, isolation by column chromatography was entirely inefficient for n ≥ 5 because of low yields and very similar R_f values. Therefore, an approach termed "sequential" DA was used to increase the yield and simplify isolation of larger oligomers as a third variant of conducting the DA of **NDIBr$_2$** and **T2** (**Scheme 1a**, conditions ii). Here, **NDBr$_2$** was reacted with an excess of 8 eq. of isolated **T2-(NDI-T2)$_n$** oligomers, allowing to prepare **T2-(NDI-T2)$_n$** with larger **n = 3, 5, 7** in over 80 % yield with respect to **NDBr$_2$** (**Table 1**, **Table S3**). Unreacted excess of **T2-(NDI-T2)$_n$** was easily recovered by selective Soxhlet extraction or CC as detailed in the Supporting Information. This sequential DA defined n = 7 as the largest accessible oligomer length for the **T2-(NDI-T2)$_n$** series. As will be discussed in due course, the opto-electronic properties for this chain length will have converged, rendering this oligomer series highly suitable to bridge the gap between small molecules and disperse polymers. Notably, all six oligomers **T2-(NDI-T2)$_n$** (**n = 1-5, 7**) were monodisperse according to size exclusion chromatography (SEC), gave single peaks in MALDI-ToF MS with distinct isotope patterns (**Figure 1**, **Figure S3**), and exhibited well-defined NMR spectra (see Supporting Information), showcasing their high purity and defect-free structure. Thus, the combination of oligomerization and sequential DA gives access to oligomers **T2-(NDI-T2)$_n$** with **n ≤ 7**. DA oligomerization and sequential DA described above can be performed at the gram scale without BBV and compromising yield.

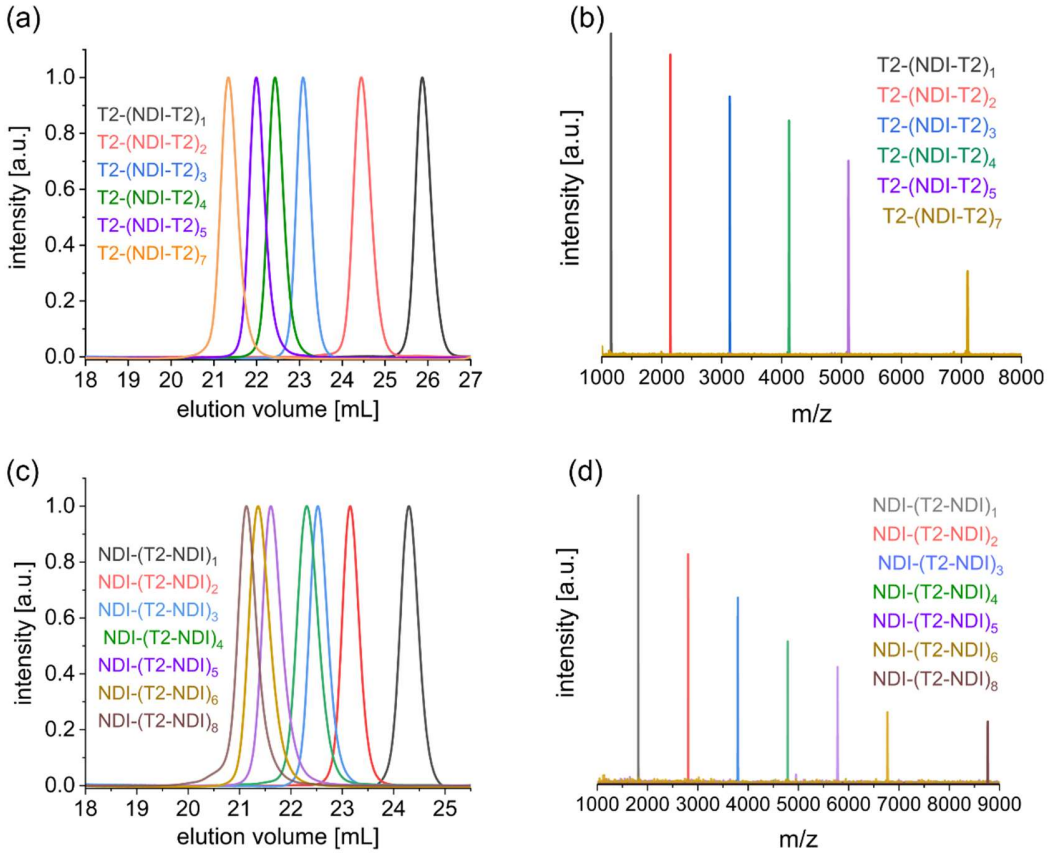

Figure 1. SEC curves (a, c) and MALDI-ToF MS (b, d) spectra of oligomers **T2-(NDI-T2)$_n$** (a, b) and **NDI-(T2-NDI)$_n$** (c, d).

Well-defined **T2-(NDI-T2)$_n$** oligomers were end capped with **NDIBr** in quantitative yield, furnishing a second series of NDI-terminated oligomers **NDI-(T2-NDI)$_n$** (**n = 1 - 8**) (**Scheme 1b**, conditions iii)). Unexpectedly, this reaction required extensive optimization to eliminate products formed by non-selective C-H arylation at T2 units (**Table S4**, **Figure S4**). Such reactions were so far not observed in extensively optimized reaction protocols by our group.[42,49–51] To eliminate unselective C-H activation, we reduced the equivalents of **NDIBr** from 2.2 to 2.0, the reaction temperature from 90 °C to 70 °C and increased the reaction time. Under these conditions, unselective C-H activation was suppressed but mono-substitution appeared. We next retained 70 °C and increased the catalyst loading to 3 mol%, where mono-substitution was mostly eliminated but unselective C-H activation reappeared. Finally, the additive pivalic acid (PivOH) was replaced by the more bulky neodecanoic acid (NDA)[52] resulting in complete elimination of unselective CH-activation. The effect of preventing β-arylation by NDA due to steric hindrance is known from other thiophene monomers.[52] Here, however, we found that the combination of using NDA, a precisely controlled amount of **NDIBr**, low temperature and low catalyst loading were crucial to eliminate unselective C-H activation and maximize yield (see conditions iii) in Scheme 1).

Thus, under fully optimized conditions for quantitative conversion of T2 end groups, quantitative yield of **NDI-(T2-NDI)$_n$** (**n = 1-8**) was achieved, with a few % lost product during work-up (**Scheme 1a**). Notably, purification of NDI-terminated oligomers was accomplished without column chromatography by precipitation following Soxhlet extraction/reprecipitation. All resulting NDI-terminated oligomers were monodisperse and had high purity as evidenced by SEC (**Figure 1**), MALDI-ToF MS (**Figure 1**, **Figure S5**), and NMR spectroscopy (see Supporting Information).

Table 1. Summary of molecular, optical, and thermal data of the oligomers

Oligomer	yield [%]	M_{MALDI} [Da]	$M_{n,SEC}$ [c] [kDa]	λ_{max} [nm][d]	LUMO [eV][e]	HOMO [eV][e]	T_m [°C]	T_c [°C]	ΔH_m [J/g]	ΔH_c [J/g]
T2-(NDI-T2)$_1$	47 [a], 92 [b]	1156.6	1.4	573	-3.74	-5.51	113.0	88.8	27.6	32.8
T2-(NDI-T2)$_2$	14 [a]	2144.4	2.3	594	-3.74	-5.55	162.7	133.8	30.1	31.0
T2-(NDI-T2)$_3$	9 [a], 93 [b]	3132.9	3.7	603	-3.74	-5.53	193.8	182.1	21.5	20.3
T2-(NDI-T2)$_4$	4 [a]	4121.9	5.0	616	-3.73	-5.52	222.7	207.0	22.6	22.7
T2-(NDI-T2)$_5$	81 [b]	5112.7	6.2	616	-3.73	-5.52	236.4	226.8	25.0	24.0
T2-(NDI-T2)$_7$	80 [b]	7097.5	9.0	621	-3.73	-5.51	260.0	253.4	25.4	25.1
NDI-(T2-NDI)$_1$	98	1815.5	1.9	556	-3.71	-5.51	103.3	46.1	17.4	7.5
NDI-(T2-NDI)$_2$	98	2805.0	3.7	590	-3.71	-5.58	162.9	106.7	26.0	14.2
NDI-(T2-NDI)$_3$	98	3793.3	4.8	602	-3.72	-5.58	168.8	160.3	20.6	19.3
NDI-(T2-NDI)$_4$	95	4783.3	5.8	611	-3.72	-5.57	197.8	192.5	19.2	21.1
NDI-(T2-NDI)$_5$	97	5752.2	7.6	615	-3.72	-5.56	219.0	213.9	23.6	22.7
NDI-(T2-NDI)$_6$	97	6771.7	8.8	615	-3.72	-5.56	236.0	232.3	22.4	19.3
NDI-(T2-NDI)$_8$	97	8760.4	10.0	622	-3.74	-5.50	258.5	254.9	20.5	20.5
IDT-(NDI-IDT)$_1$	39 [a]	2636.7	2.7	674	-3.72	-5.35	-	-	-	-
IDT-(NDI-IDT)$_2$	14 [a]	4366.5	4.5	689	-3.72	-5.35	-	-	-	-
IDT-(NDI-IDT)$_3$	5 [a]	6100.6	6.0	697	-3.72	-5.34	-	-	-	-
IDT-(NDI-IDT)$_4$	n.d.	7844.3	7.4	697	n.d.	n.d.	-	-	-	-

[a] isolated yields from DA oligomerization; [b] isolated yields from sequential DA; [c] dispersity (Đ) is 1.0 for all oligomers except for the octamer, where $Đ$= 1.03 is caused by aggregation. [d] λ_{max} in 1-chloronaphthalene; [e] LUMO and HOMO energy levels are calculated from solution cyclic voltammetry (CV) measurements in 1,2-chlorobenzene (*o*-DCB) with ferrocene as external standard as detailed in the SI. Thermal properties, including melting/crystallization temperature and corresponding enthalpies are taken from second melting and first cooling curve of the DSC traces taken at 10 K/min.

Reaction scope and strategies to modulate crystallization

Crystallinity of materials is one of the important aspects controlling thin film microstructure and thus device performance in OPV.[41,53] On the one side, organic semiconductors

with high crystallinity often show improved charge transport and thus better performance.[41,54] In terms of photovoltaic applications, OPV devices made from binary blends in which one or even two components are highly crystalline may suffer from fast phase separation and large domain sizes that come along with strongly reduced interfacial area and finally low performance. [55,56]

More important for OPV blends is the ability of acceptors to form network structures in the presence of a p-type material, as seen for the high performance non-fullerene acceptor Y6.[5,6,55] Such network formation may be facilitated by acceptor molecules with a less linear shape. In order to find simple synthetic strategies towards oligomers with reduced or suppressed crystallinity, we explored whether control over the herein observed unselective CH activation at positions other than α-hydrogens of **T2** could be attained.

To this end, we investigated the reaction of 4.0 eq **NDIBr** with 1.0 eq **T2-NDI-T2** at high temperature and high catalyst loading. Two main fractions were isolated. According to MALDI-ToF MS, these were found to be a complex mixture of several molecules with varying numbers of NDI units, despite each showing one spot on the TLC plate (**Figure S6**). Owing to the various possibilities of non-selective CH activation of **T2** (**Figure 2**, top) and the resulting difficulties in purification as well as the challenging characterization of mixtures by NMR spectroscopy, we simplified the reaction using **NDI-T2-NDI** (**Scheme 1c**). MALDI-ToF MS of the crude reaction mixture (**Figure 2**) indicated unreacted **NDI-T2-NDI** (**Figure 2**, peak **6**) and **NDIBr** (**Figure 2**, peak **3**) along with m/z values corresponding to NDI (debromination, **Figure 2**, peak **1**), **NDI-OH/Piv** (nucleophilic substitution, **Figure 2**, peak **2**/**4**)[42,51], **NDI-NDI** (homocoupling, **Figure 2**, peak **5**), single additional NDI-substitution **NDI-T2(NDI)$_1$-NDI** (**Figure 2**, peak **7**) and twice additional NDI-substitution **NDI-T2(NDI)$_2$-NDI** (**Figure 2**, peak **8**). MALDI-ToF MS of two isolated main products exhibited single peaks with the same m/z value of 2640.097 Da. These values correspond to one additional NDI substitution, which must have occurred at a C-H position of **T2** other than α. Apart from these two fractions, trace amounts of **NDI-T2(NDI)$_2$-NDI** were also isolated. Since MALDI-ToF MS alone is not able to provide the position of non-selective CH activation, we analyzed them with NMR spectroscopy.

The ^{1}H NMR spectra of the two **NDI-T2(NDI)-NDI** fractions show that the additional NDI substitution on one thiophene ring results in a singlet for the remaining proton, while the two protons of the other thiophene ring of the T2 unit give two doublets (**Figure 3a**, **b**, **Figures S7-10**). The substitution pattern (β vs. γ, see Figure 2 top) was elucidated from through-space correlations between thiophene and NDI protons observed in the ROESY spectra (**Figures S8** and **S10**). H_2 in **NDI-T2(β-NDI)-NDI** shows correlation only to one NDI ring (β-NDI), whereas H_1 in **NDI-T2(γ-NDI)-NDI** correlates to α-NDI and γ-NDI. In summary, the first fraction corresponds to the product formed by β-arylation of the internal T2 unit, giving **NDI-T2(β-NDI)-NDI**, while the second fraction is γ-substituted **NDI-T2(γ-NDI)-NDI** containing trace amount of unreacted **NDI-T2-NDI**. With ^{1}H NMR assignments from isolated isomers (**Figure S7-10**), the ^{1}H NMR spectroscopic analysis of the crude reaction mixture indicated a molar ratio β/γ- substitution of 36/64 (**Figure S11**).

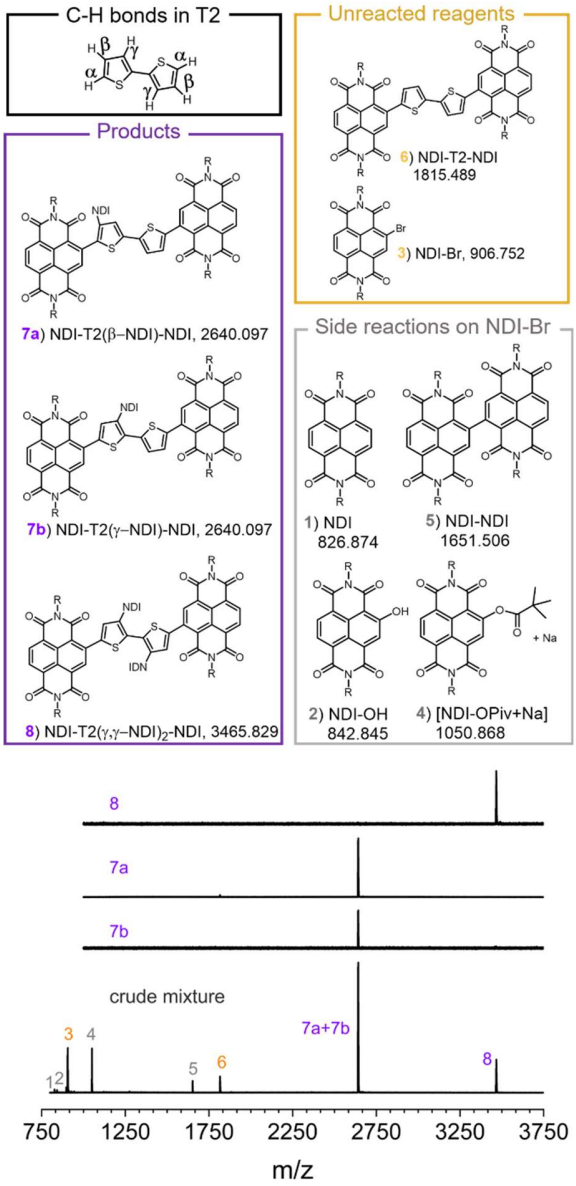

Figure 2. MALDI-ToF mass spectra of the reaction **Scheme 1c**: crude reaction mixture and isolated products (**7a**, **b** and **8**). Corresponding chemical structure and m/z values of each peaks are shown above. R: 2-octyldodecyl.

Obviously, under the conditions applied here, γ-arylation is more favourable, probably due to lower sterical hindrance. However, the reaction is not very selective overall. Even though the β-position may be more reactive due to the adjacent electron withdrawing NDI unit[57,58], the effect of steric hindrance possibly overrides electronic factors. This is more evidently seen by the symmetric disubstituted product **NDI-T2(γ, γ-NDI)$_2$-NDI**, where both γ-positions have reacted. Its structure was confirmed by ^{1}H NMR (**Figure 3c, Figure S12**) and ROESY correlations of the thiophene proton to α-NDI and γ-NDI (**Figures S13-15**). Steric crowding in **NDI-T2(γ, γ-NDI)$_2$-NDI** leads to hindered rotation of the

γ-NDI as evidenced by line broadening of both the thiophene proton (H_1) and the γ-NDI proton (H_5) adjacent to the substituent. Variable temperature measurements leading to line narrowing with increasing temperature (**Figure S15**) support this conclusion.

To support the strategy of a reduced or even suppressed crystallization, we performed differential scanning calorimetry (DSC) of these β/γ-substituted products. All purified isomers with additional NDI units at non-α-positions did not show any melting/crystallization transitions (**Figure S16**), indicating that such bulk substituents effectively suppress crystallinity of the oligomers entirely. Glass transition temperatures (T_g) of around 9 °C and 17 °C were observed for **NDI-T2(β-NDI)-NDI** and **NDI-T2(γ-NDI)-NDI**, respectively (**Figure S16**).

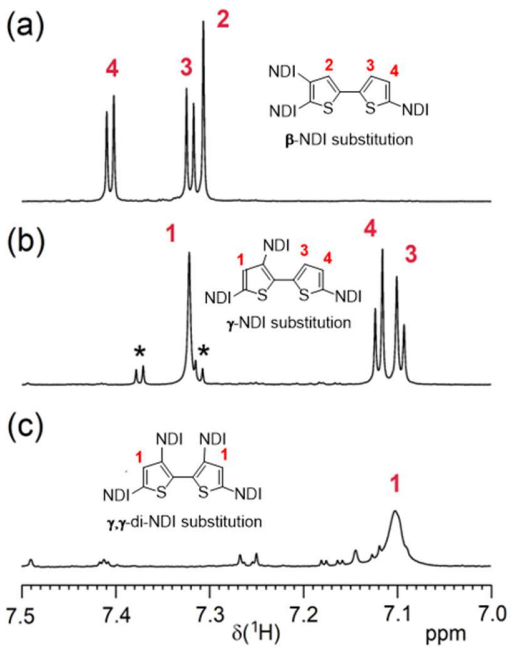

Figure 3. ^{1}H NMR spectra (region of thiophene protons) of (a) **NDI-T2(β-NDI)-NDI**, (b) **NDI-T2(γ-NDI)-NDI** and (c) **NDI-T2(γ, γ-NDI)$_2$-NDI** (solvent: CD_2Cl_2). The asterisks mark signals of a trace of **NDI-T2-NDI**.

In addition to branching reactions, we further explored the reaction scope by using different thiophene comonomers. Here, we used bulky hexylphenyl-substituted indacenodithiophene (**IDT**) as a popular building block[55,59] to modulate crystallization and to demonstrate the generality of our approach leading to well-defined, symmetrically IDT-terminated oligomers **IDT-(NDI-IDT)$_n$** with **n = 1-4** (**Scheme 1d**, for SEC and MALDI-ToF MS spectra see **Figure S17**, for NMR spectra see **SI**). Due to the observed inferior reactivity of **IDT** compared to **T2**, an increased catalyst loading of 2% was required to achieve full conversion. Applying the already optimized DA end capping protocol with **NDIBr** furnished **NDI-(IDT-NDI)$_2$** in quantitative yield and with defect-free structure (**Scheme S2**, **Figure S17**). All IDT-containing oligomers independent of chain length and termination are fully amorphous as discussed further below.

Evolution of electronic and optical properties with chain length

To gain insight into the electronic structure of **T2-(NDI-T2)$_n$** and **NDI-(T2-NDI)$_n$** oligomers of varying length, simulations were performed based on density functional theory (DFT) at the CAM-B3LYP/6-311G(d, p) level.[60–62] For details of the methods, see the Experiments/Methods section below. In general, the lowest unoccupied molecular orbital (LUMO) energy levels of the oligomers are mostly related to the LUMO of **NDI** and the highest occupied molecular orbital (HOMO) energy levels mostly to the HOMO of **T2**. This affected not only the orbital shapes but also their energies as depicted in **Figure S18**. It can already be seen for **NDI-T2-NDI** that the LUMO is partially delocalized over both **NDI** units, while the HOMO of **T2-NDI-T2** is delocalized over both **T2** units.

As shown for **T2-(NDI-T2)$_7$** in **Figure 4a** (for data on other shorter oligomers see **Figure S19**), delocalization of the frontier molecular orbitals rapidly converges for longer oligomers: the HOMO is mainly delocalized over two T2 units with slight contributions on a third unit and the LUMO is delocalized only over two NDI units. It needs to be mentioned that according to the number of NDI and T2 units, the oligomers show further molecular orbitals that are superpositions of the units' HOMOs and LUMOs.[63] For instance, in T2-(NDI-T2)$_4$ the HOMO levels of the five T2 units lead to the HOMO to HOMO-4 states within an energy range of 200 meV. Accordingly, the LUMO levels of the four NDI units lead to the LUMO to LUMO+3 states within an energy range of only 100 meV. It can be expected that these molecular orbitals are to some extend dynamically degenerated considering the shallow energy landscape of the oligomers with a multitude of local energy minima.

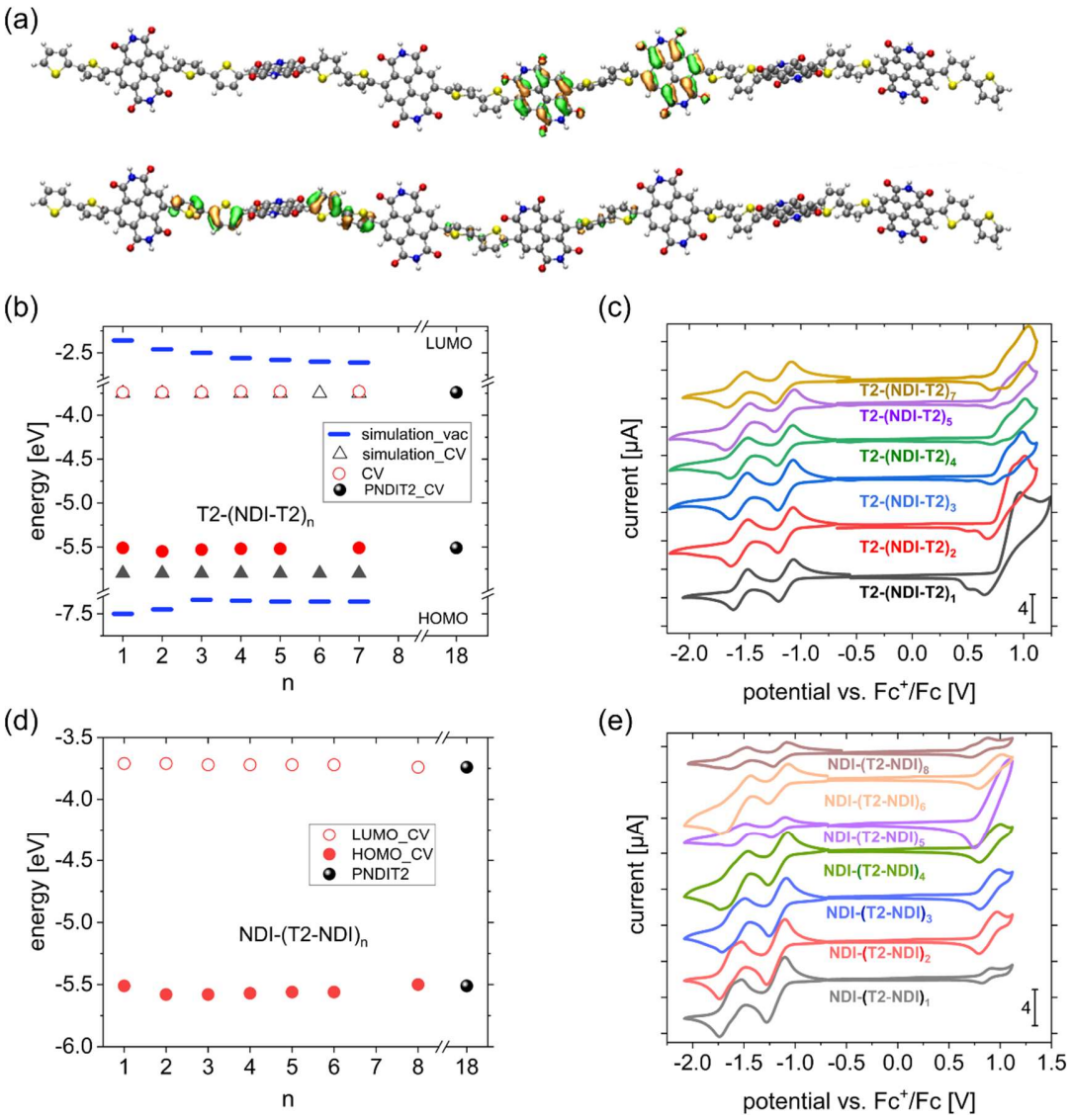

Figure 4. Frontier molecular orbitals (LUMO top, HOMO bottom) of **T2-(NDI-T2)$_7$** (a): the delocalization of the HOMO is limited to two to three T2 units, whereas the LUMO is only limited to two NDI units. Molecular energy levels (b, d) and CV curves (c, e) of **T2-(NDI-T2)$_n$** (b, c) and **NDI-(T2-NDI)$_n$** (d, e) oligomers. Values from simulations are in vacuum (blue sticks) or in *o*-DCB solution (triangle). Experimental energy values of all oligomers and additionally PNDIT2 (black sphere) are taken from CV measurements in solution (0.1 M [^{n}Bu$_4$N][PF$_6$] in *o*-DCB).

The fast convergence of the orbital delocalization of the frontier molecular orbitals with chain length also leads to the almost identical energy levels irrespective of chain length (**Figure 4b**). Similar to the simulated energy levels in vacuum (**Figure 4b**, blue sticks), reduction potentials from differential pulse voltammetry (DPV) profiles (**Figure S20**) show at first subtle but steady decrease with chain length until n = 4 and then saturate, giving a similar value for the rest of the oligomers irrespective of chain length and end group. The energy levels from solution cyclic voltammetry (CV) measurements (**Figure 4b, d** (circle), **c** and **e**, **Table S5**) and simulations (**Figure 4b** (triangle), **Table S6**) gave rather similar energy levels for all oligomers regardless of chain length. Overall, T2-terminated oligomers have a slightly lower LUMO energy level than NDI-terminated oligomers, whereas from simulation similar values were calculated (**Table S6**). Nevertheless, LUMO levels of around -3.74 eV are extracted for **T2-(NDI-T2)$_n$**, which is almost identical to that of **PNDIT2** measured under the same condition (**Figure 4b**). HOMO energy levels are instead not affected by terminal groups, all **T2-(NDI-T2)$_n$** and **NDI-(T2-NDI)$_n$** oligomers give almost identical values. HOMO energy levels from simulation are lower by 300 meV (**Figure 4b**, **Table S6**), but again similar for all oligomers. Theoretical gas phase HOMO and LUMO energy levels (**Table S6**) slightly shift into lower energy with increasing chain length due to an increase in orbital delocalization. These shifts are compensated by an increase in the ionic volume that reduces the polarization shift by the solvent.[64]

The **IDT-(NDI-IDT)$_n$** oligomers as well show identical energy levels irrespective of chain length (**Figure S21**, **Table 1**, **Table S5**). LUMO levels of around -3.72 eV, which is similar to that of **NDI-(T2-NDI)$_n$** oligomers, and slightly higher HOMO levels around -5.35 eV were extracted from CV curves.

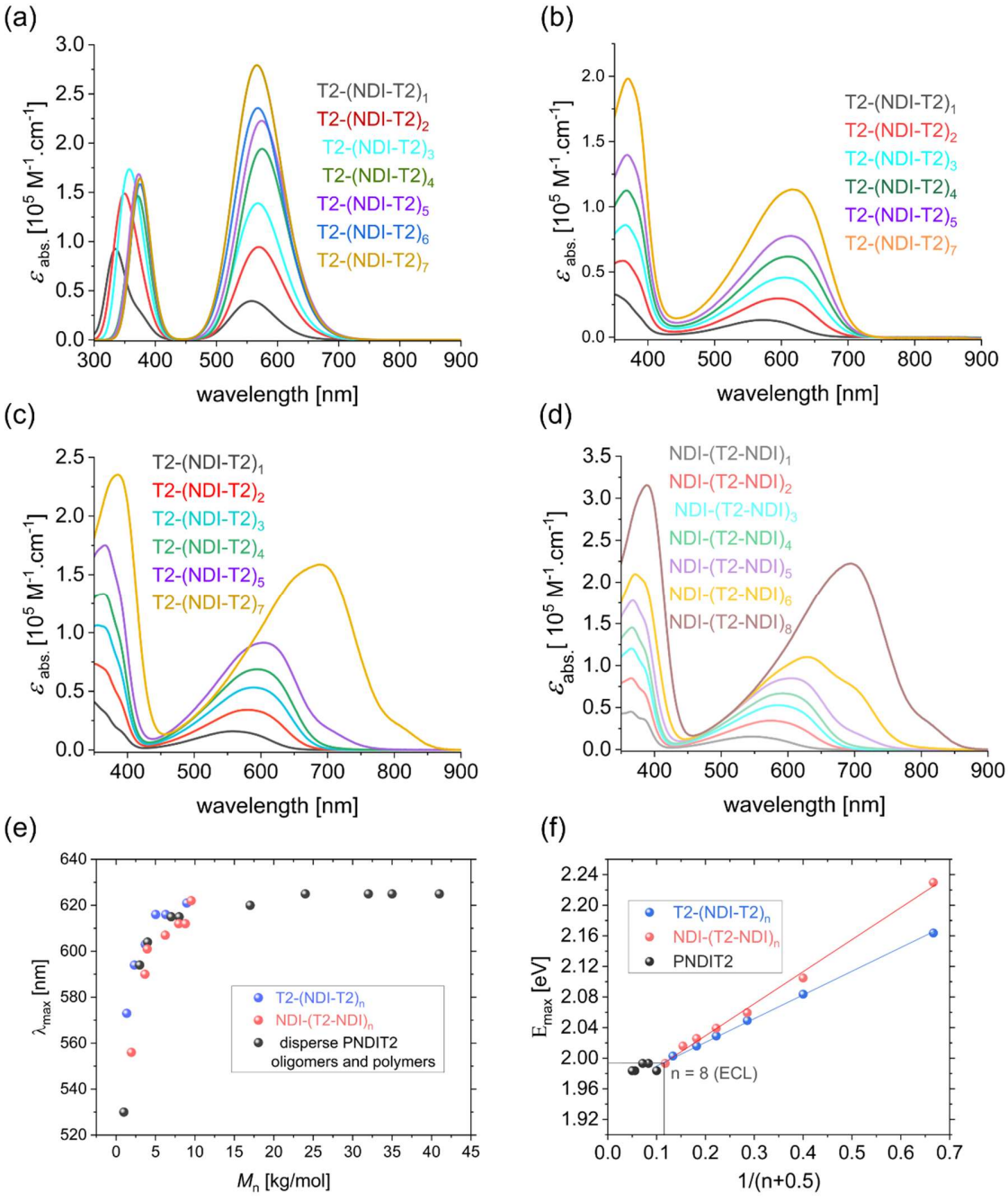

Figure 5. UV-vis absorption spectra of **T2-(NDI-T2)$_n$** (a (simulated, gas phase), b, c) and **NDI-(T2-NDI)$_n$** (d) oligomers in CN (b) and in toluene (c, d) at RT with a concentration of 0.02 g/L; Dependence of λ_{max} of the low-energy band (in CN) with M_n (e) of discrete **T2-(NDI-T2)$_n$** (blue spheres) and **NDI-(T2-NDI)$_n$** (red spheres) oligomers in comparison to disperse **PNDIT2** oligomers and polymers (black spheres, values are taken from ref[42]), all M_n values in (e) are from SEC measurements using chloroform as solvent. Correlation between maximum absorption energies E_{max} and chain length (f) to determine effective conjugation length (ECL), chain length of **PNDIT2** are from NMR spectroscopy.

To further determine the effective conjugation length (ECL) of aggregation in solution, UV-vis absorption spectroscopy was carried out in 1-chloronaphthalene (CN) (**Figure 5b**, **Figure S22**) which leads to molecularly dissolved solutions independent of oligomer length. To determine the onset of aggregation, toluene (**Figure 5c**, **d**) was used as well.[65] In toluene as well as in CN, the molar extinction coefficient (ε_{abs}) of both the higher energy π- π * and the lower energy charge-transfer absorption bands increases with chain length (**Table 1**) in accordance with the simulation (**Figure 5a, Figure S23**). In CN, the wavelength of the absorption maximum λ_{max} of the charge transfer band increases with oligomer length, reaching 622 nm for **NDI-(T2-NDI)$_8$** and 621 nm for **T2-(NDI-T2)$_7$**. These values are very close to **PNDIT2** with λ_{max} of 622-625 nm (**Figure 5e**). Correlation between maximum absorption energies $E_{max} = \frac{hc}{\lambda_{max}}$ (where h is the Plank constant, c is speed of light) and chain length of the oligomers in comparison to that of PNDIT2 indicates that ECL for this system, irrespective of terminating groups, is around n = 8 (**Figure 5f**). In toluene, the aggregation onset was found to be n = 5 for both T2- and NDI-terminated oligomers with raising of an absorption shoulder at lower energy of 720 nm corresponding to so called 'aggregate I'[12,65]. Aggregate II on the other hand occurs from n = 6. Intensity of both aggregates increases with chain length and becomes very distinct for the longest oligomers (**Figure 5c**, **d**). The spectrum of both **T2-(NDI-T2)$_7$** and **NDI-(T2-NDI)$_8$** resembles to that of PNDIT2 with slightly shorter λ_{max} for aggregate I (**Figure S24**), indicating that it can represent the analog polymer.[42,65] **T2-(NDI-T2)$_n$** oligomers overall show higher ε_{abs}, larger λ_{max}, and stronger aggregation than **NDI-(T2-NDI)$_n$** oligomers of same chain length.

For **IDT-(NDI-IDT)$_n$** oligomers, a similar trend of an increasing λ_{max} and intensity with oligomer chain length was observed both in CN and toluene (**Figure S25**). However, the increase in λ_{max} is very minor. Additionally, absorption features remain almost the same in both solvents due to the absence of aggregation in herein tested solvents. Therefore, for this system we assume that ECL has already been reached.[59]

Crystallization and structure formation

Next, we turned our attention to crystallization and structure formation of these oligomers as a function of chain length, end groups, and comonomers. First DSC measurements were performed on bulk samples. For both T2- and NDI-terminated oligomers, melting (T_m) and crystallization temperatures (T_c) increased with oligomer length (**Figure 6 a-d**) and furthermore did not reach saturation to the values of PNDIT2, which usually melts at T_m> 300 °C.[42] NDI-end capped oligomers instead delivered slightly lower T_m and T_c values, larger supercooling for n= 1,2, and multiple phase transitions in comparison to T2-terminated oligomers of the same chain length (**Table 1**). All oligomers showed much higher melting (ΔH_m) and crystallization (ΔH_c) enthalpies > 20 J/g than their polymeric analogues, from which values < 10 J/g depending on MW and synthetic methods are common.[42] While this is typical for small molecules as compared to semicrystalline polymers[66], integration of broad melting peaks seen with disperse low molecular weight semi-crystalline polymers can be challenging, leading to an underestimation of crystallinity.[42,67] ΔH_m of **T2-(NDI-T2)$_n$** and **NDI-(T2-NDI)$_n$** oligomers increase first with chain length and then become slightly lower from n = 3 and reach a rough plateau (**Figure 6e**, **f**). Overall, **T2-(NDI-T2)$_n$** oligomers have higher enthalpies than **NDI-(T2-NDI)$_n$**. This is in line with the observed stronger aggregation for **T2-(NDI-T2)$_n$** than NDI-terminated **NDI-(T2-NDI)$_n$** oligomers in solution.

Modulating and controlling crystallinity is important for solid state properties of organic semiconductors to be used in thin film solar cells or transistors.[41,53] The crystallinity of these oligomers can be largely suppressed by using thiophene comonomers with bulky substituents such as phenylhexyl-substituted **IDT** motifs[59]. From conventional DSC measurements on powder samples of **IDT-(NDI-IDT)$_n$**, melting and crystallization events were absent. Instead, these oligomers showed T_g values that increase from 74 °C, to 127°, and to 145 °C for n= 1, 2, 3 (**Figure S26**). End capping **IDT-(NDI-IDT)$_n$** oligomers with NDI further increased T_g as evidenced for **NDI-(IDT-NDI)$_2$**, which has T_g at around 114 °C (**Figure S27**).

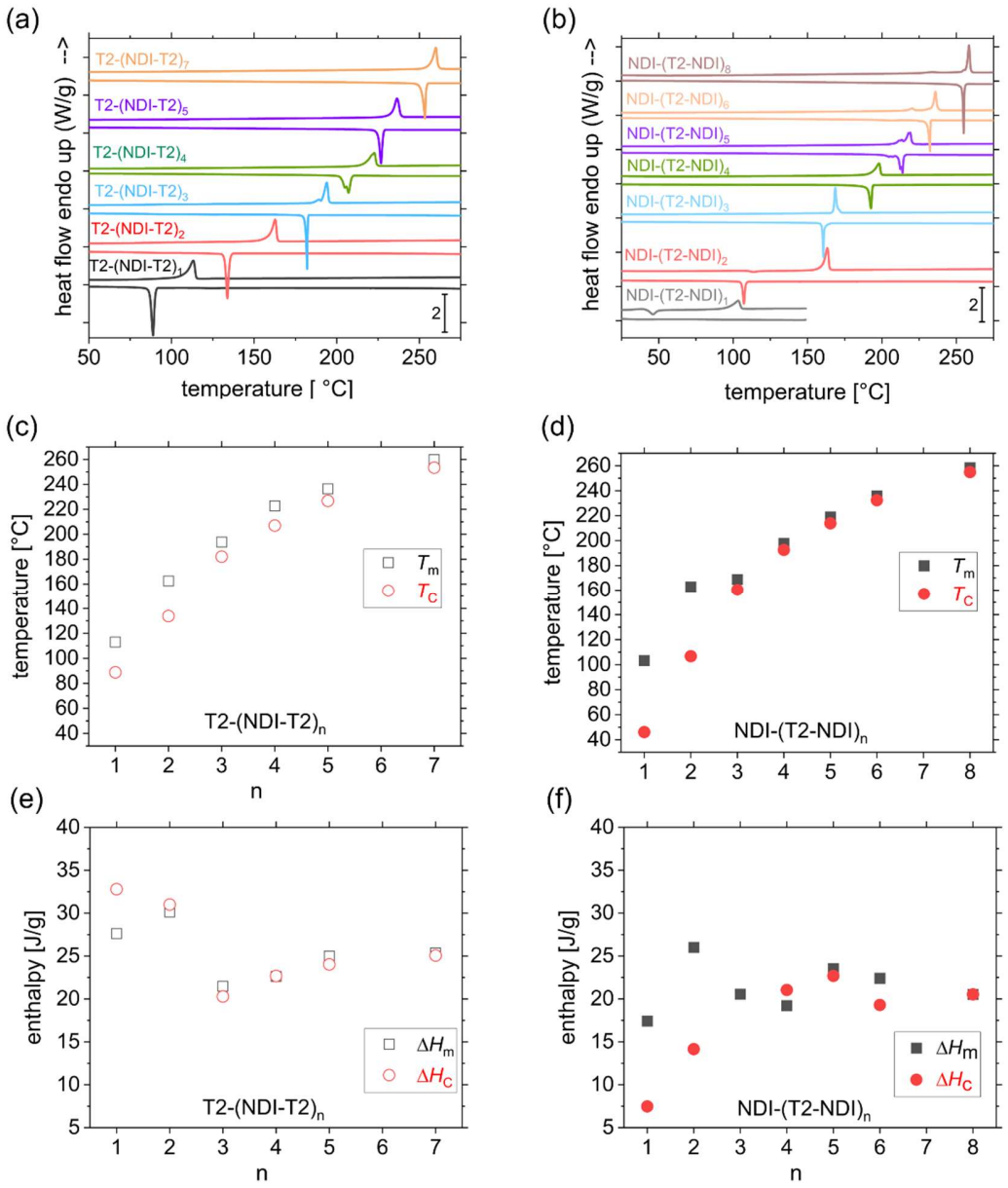

Figure 6. Thermal properties and crystallization behavior of the oligomers: DSC curves (a, b), melting and crystallization temperatures (T_m, T_c) (c, d) and corresponding enthalpies (e, f) of **T2-(NDI-T2)$_n$** (a, c, e) and **NDI-(T2-NDI)$_n$** (d, c, f).

Finally, more insight into molecular packing of T2- and NDI-terminated oligomers was obtained from transmission electron microscopy (TEM) on oriented thin films given the difficulty to grow single crystals suitable for classical X-ray diffraction analysis. Oriented films of **T2-(NDI-T2)$_n$** and **NDI-(T2-NDI)$_n$** were prepared by casting chlorobenzene solutions onto oriented poly(tetrafluoroethylene) (PTFE) substrates followed by melt-crystallization. The structure was analyzed by electron diffraction and comparison was made with the known structure of the polymer PNDIT2. PNDIT2 exists in two crystalline forms called form I and form II depending on whether the NDI and bithiophene are segregated (form I) or mixed-stacked (form II).[68] **Table 2** collects the main structural information gained from electron diffraction on oriented thin films shown in **Figure 7**. First, for n = 2, both T2- and NDI-terminated oligomers display a crystalline structure with electron diffraction patterns quite different from the polymer. The patterns are characteristic of the coexistence of two crystal populations with two different in-plane orientations possibly induced by 1D-epitaxy on PTFE.[69] For **T2-(NDI-T2)$_2$** the ED pattern suggests that the molecules are oriented end-on to the PTFE substrate (long axis of oligomer parallel to substrate normal). **NDI-(T2-NDI)$_2$** displayed a polymorphism similar to that of the polymer with the characteristic UV-vis-NIR spectral signatures of form I and form II, form II being the stable one (see **Figure S28**, note the well-defined vibronic structure for the oriented form II-like films of **NDI-(T2-NDI)$_2$**). Second,

for longer oligomers (n = 3-5), ED patterns become similar to the oriented polymer with the oligomer long axis parallel to the PTFE chain direction. The well-defined molecular length of oligomers translates to corresponding lamellar phases with a well-defined periodicity, as observed classically for paraffines.[70] The intensities of the h k l reflections along the c axis are modulated by the finite lamellar periodicity (additional reflections pointed by red arrows in **Figure 7b**). The lamellar structure is also seen in the low dose high resolution TEM (HR-TEM) images for **NDI-(T2-NDI)$_n$** with n = 4 and n = 5 (**Figure S29**). As expected, the total lamellar periodicity scales with the length of the oligomer, albeit the measured values (7.4 nm and 9.1 nm for n = 4 and 5, respectively) are slightly larger compared to the lengths of the extended molecules, which are 6.4 nm and 7.8 nm, respectively.[70] In strong contrast to paraffines showing highly crystalline lamellar phases, the lamellae of **NDI-(T2-NDI)$_n$** seem to be more disordered, explaining at least in part the limited order of the obtained ED patterns. For n ≥ 3, the diffraction patterns of oriented oligomer films became similar to that of the polymer PNDIT2. Form II (mixed stacking of **T2** and **NDI**) is evidenced for **NDI-(T2-NDI)$_n$** with n = 3-6 oligomers with typical lattice parameters that are close to those of the polymer (see **Table 2**).

T2-(NDI-T2)$_n$ oligomers show also evidence for polymorphism. The only form II is observed after melt-crystallization for n = 3, whereas for n = 4 the monoclinic form I coexists with form II. This is an interesting finding since it may suggest that the polymorphism of PNDIT2 and oligomers could be influenced by the chemical nature of the terminal T2 or NDI units. For **NDI-(T2-NDI)$_n$** oligomers, some variations of the lattice parameters are observed, especially in the long-axis direction of the molecule (c-axis). Also interesting is the fact that short oligomers with n = 2 tend to grow end-on to the PTFE substrate while for all other oligomers, the long molecular axis tends to align parallel to the PTFE chain direction as for the polymer.

Table 2. Main structural data of NDI-(T2-NDI)$_n$ and T2-(NDI-T2)$_n$ thin films prepared by melt-crystallization onto oriented PTFE substrates in comparison to PNDIT2.

h k l *	NDI-(T2-NDI)$_n$ d_{hkl} (Å)				T2-(NDI-T2)$_n$ d_{hkl} (Å)			polymer d_{hkl} (Å)
	n = 2	n = 3	n = 4	n = 5	n = 2	n = 3	n = 4	PNDIT2
lamellar period (nm) c axis			7.2±0.2	9.1±0.2		-	4.6±0.2	-
polymorph	-	form ll	form II	form II	-	form II	form I + II	form II
contact plane	-	edge-on	face-on edge-on	face-on edge-on	-	edge-on	face-on edge-on	
1 0 0	21.8	25.1	24.8	25.1	-	-	24.6	24.7
2 0 0	-	12.53	12.40	12.53	-	-	-	12.4
0 0 1	14.2	13.0	13.0	13.54	13.6		14.14	14.1
0 0 2	7.29	7.20	7.14	7.19	6.8	7.25	7.1	7.1
0 0 4	-	3.60	3.59	3.60	-	3.60	3.55	3.56
1 0 -2	-	-	-	-	-	-	7.25	-
1 0 1	-	12.4	12.4	12.4	-	-	-	12.85
0 1 2	-	5.36	5.34	5.36	-	-	-	-
0 2 0	-	3.98	3.96	4.02	-	3.92	3.93	4.0
0 2 1	-	-	3.76	-	-	-	-	-

* Indexation corresponds to form II of **PNDIT2**. For the oligomers, the c axis period is different from that in the polymer and thus indices must be renumbered considering the total lamellar period corresponding to the c axis length.

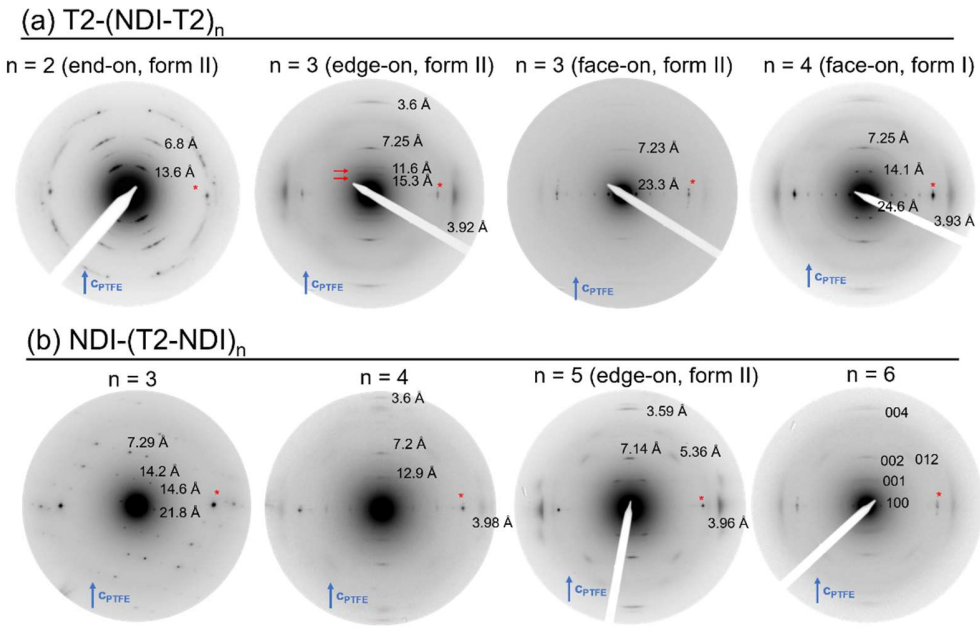

Figure 7. Representative electron diffraction patterns of oriented thin films of **T2-(NDI-T2)$_n$** (a) and **NDI-(T2-NDI)$_n$** (b) obtained by melt-crystallization on oriented PTFE substrates. The 100 reflection at 4.9 Å of PTFE is indicated by a red asterisk. Note for the **NDI-(T2-NDI)$_3$** that the films consist of two populations of oriented crystals with c either parallel or perpendicular to c_{PTFE}. The direction of the PTFE chains is highlighted by an arrow.

Conclusion

We have developed an efficient synthetic approach enabling the preparation of a large number of discrete n-type oligomers on the gram scale. The oligomers comprise naphthalene diimide (**NDI**) and thiophene-based comonomers, exemplified by bithiophene (**T2**) and indacenodithiophene (**IDT**). By virtue of combining several variants of optimized protocols of direct arylation (DA) oligomerization, sequential DA, and DA end capping, the series **T2-(NDI-T2)$_n$**, **NDI-(T2-NDI)$_n$**, and **IDT-(NDI-IDT)$_n$** were prepared for n ≤ 8. Key to the success of the presented synthetic procedure is the ability to make fully T2-terminated oligomers. In all oligomers, molecular energy levels are not affected by chain length as evidenced from both experiments and simulations. **T2-(NDI-T2)$_7$** and **NDI-(T2-NDI)$_8$** being the longest oligomers exhibit similar absorption, aggregation, and energy levels to the analogous polymer PNDIT2. For both **T2-(NDI-T2)$_n$** and **NDI-(T2-NDI)$_n$** oligomers, their T_m and T_c increase with chain length, but are still lower than for PNDIT2 in all cases. However, melting and crystallization enthalpies are much larger, pointing to higher crystallinities than polymeric analogs. **IDT-(NDI-IDT)$_n$** and **NDI-(IDT-NDI)$_n$** oligomers are amorphous under the experimental conditions and their T_g values increase with chain length. We also demonstrate suppression of crystallization by further reacting **NDI-(T2-NDI)$_n$** oligomers with an excess of **NDIBr** leading to branched structures. Positions of branching were identified and quantified, revealing a mixture of β- and γ-arylation with some preference for the latter. Oriented thin films of longer **T2-(NDI-T2)$_n$** and **NDI-(T2-NDI)$_n$** oligomers with n > 3 have similar electron diffraction patterns compared to PNDIT2. However, their polymorphism tends to depend on the terminal groups: NDI-terminated oligomers show form II, while T2-terminated oligomers show both form I and form II polymorphs in thin films. The synthetic approach developed here may be extended to other n-type systems to enable further structure-property relationships, provided that end group homogeneity can with optimized similarly. The herein demonstrated scalability may also give rise to the integration of discrete n-type oligomers into further polymer topologies, in which dispersity of the conjugated blocks has so far limited morphology. Studies towards these directions are underway and will be reported in due course.

Experimental/Methods

Synthesis and characterization methods. All details of the preparation and characterization are shown in the Supporting Information.

Computational methods. Density functional theory (DFT) and time-dependent DFT (TD-DFT) simulations are performed using the Gaussian 16 package[71]. As DFT is known to be impacted by the delocalization error[72], the long-range corrected hybrid functional CAM-B3LYP is used along with its default parametrization.[60] This approach is combined with the 6-311G(d,p) basis set.[61,62]

The accuracy of the geometry optimizations is evaluated based on an analysis of the vibrational spectra for the relaxed structures. All results are based on the structures found with the lowest total energy. However, all molecules show relatively shallow energy landscapes with multiple

local minima that also satisfy the criterium of a well-defined vibrational spectrum. Accordingly, it can be expected that already at room temperature a multitude of three-dimensional conformations is accessible to the molecules leading, e.g., to the relatively broad absorption peaks measured in solution. Accordingly, the results obtained for the electronic structure of the oligomers represent only singular data points in broader distributions. Still, as the global minima analyzed resemble similar conformations, they allow to characterize the materials properties qualitatively. For all calculations, the 2-octyldodecyl side chains are substituted by hydrogen atoms to reduce the computational costs. Test calculations on **NDI-T2-NDI** and **T2-NDI-T2** did not show significant effects on the energy levels and the absorption spectra exceeding the variation in the results between different local minima.

CV measurements of the frontier energy levels in *o*-DCB are reproduced by using the integral equation formalism variant of the polarizable continuum model (IEFPCM) in combination with the D3 version of Grimme's dispersion model with Becke-Johnson damping.[73,74] The vertical ionization potential IP_{PCM} and electron affinity EA_{PCM} are determined from the energy difference of the relaxed neutral ground-state $E_0(0)$ and the ionic molecular states $E_{\pm/-}(0)$ in the same geometry

$$IP_{PCM} = E_+(0) - E_0(0), \quad (1)$$

$$EA_{PCM} = E_0(0) - E_-(0). \quad (2)$$

To account for relaxation effects, the internal reorganization energy for hole Λ_+ and electron transport Λ_- are extracted from the adiabatic potential energy surfaces for the neutral and ionic states in the relaxed neutral and ionic geometries according to

$$\Lambda_\pm = [E_0(\pm) - E_0(0)] + [E_\pm(0) - E_\pm(\pm)]. \quad (3)$$

The absolute values of the CV energy levels are calculated as follows[75]

$$IP_{CV} = IP_{PCM} - \Lambda_+/2 = |HOMO|, \quad (4)$$

$$EA_{CV} = EA_{PCM} + \Lambda_-/2 = |LUMO|. \quad (5)$$

As polarization models often do not sufficiently describe absorption in solution, the absorption spectra of the molecules are calculated in gas phase by using TD-DFT and corrected by applying an empirical energy shift of 500 meV determined from comparison with the experimental spectra. For better visualization, excited states are represented by Gaussian functions with a broadening of 20 meV resembling the broadening of the experimental absorption features.

Molecular Packing. Oriented thin films of oligomers were prepared on friction-transferred poly(tetrafluoroethylene) substrates deposited on clean glass substrates. The method of preparation of oriented PTFE is described in reference[76]. Thin films of oligomers were prepared by casting from 6 g/L solutions in chlorobenzene at 125°C. The films on PTFE were then transferred to a Linkam THMS-600 hot stage connected to a TMS-94 temperature controller under N_2 atmosphere. The samples were first molten at a temperature slightly above T_m for 1 min and then cooled down to room temperature at 30°C/min.

For TEM analysis, the films were coated with a thin amorphous carbon layer using an Auto 306 Edwards evaporator.

Oriented parts of the films were selected under a Leica DMR-X polarized light microscope and floated on diluted 5 wt.-% aqueous solution of HF and subsequently transferred to TEM copper grids. TEM was performed in low dose using a 120kV CM12 microscope equipped with a MVIII (Soft Imaging Systems) CCD camera.

ASSOCIATED CONTENT

Supporting Information. Materials used, detailed synthetic procedures, further theoretical and structural characterization including NMR spectroscopy, elemental analysis, MALDI-ToF MS, UV-vis spectroscopy, CV, and DSC are given in the supporting information. This material is available free of charge via the Internet at http://pubs.acs.org.

AUTHOR INFORMATION

Corresponding Author

* Michael Sommer: michael.sommer@chemie.tu-chemnitz.de

Present Addresses

†If an author's address is different than the one given in the affiliation line, this information may be included here.

Author Contributions

The manuscript was written through contributions of all authors. All authors have given approval to the final version of the manuscript.

Funding Sources

MS and RM acknowledge funding from the Deutsche Forschungsgemeinschaft (DFG) (project SO 1213/8-2). FO thanks the DFG for funding (project OR 349/3-1 and the Cluster of Excellence e-conversion (grant no. EXC2089)).

Notes

Any additional relevant notes should be placed here.

ACKNOWLEDGMENT

RM and MS are thankful to R. Weber for performing SEC, to R. Hertel and M. Raisch for performing DSC, and to D. Adamczak for providing IDT. Grants for computer time from the Zentrum für Informationsdienste und Hochleistungsrechnen of TU Dresden and the Leibniz Supercomputing Centre in Garching are gratefully acknowledged.

ABBREVIATIONS

NDI, naphthalene diimide; T2, bithiophene; OFETs, organic field-effect transistors; OPV, organic photovoltaics; poly{[N,N′-bis(2-octyldodecyl)-naphthalene-1,4,5,8-bis(dicarboximide)-2,6-diyl]-alt-5,5′-(2,2′-bithiophene)}, PNDIT2; BBV, batch-to-batch variations; T_g, glass transition temperature; DA, direct arylation; DAP, direct arylation polymerization; TLC, thin layer chromatography; CC, column chromatography; PivOH, pivalic acid; NDA, neodecanoic acid; MALDI-ToF MS, matrix-assisted laser desorption ionization time-of-flight mass spectrometry; λ_{max}, absorption maximum; SEC, size exclusion chromatography; NMR, nuclear magnetic resonance; ROSEY, rotating frame overhauser enhancement spectroscopy; ECL, effective conjugation length; ε_{abs}, the molar extinction coefficient; M_n,

number average molecular weight; CN, 1-chloronaphthalene; DFT, density functional theory; TD-DFT, time-dependent DFT; LUMO, lowest unoccupied molecular orbital; HOMO, highest occupied molecular orbital; CV, cyclic voltammetry; DPV, differential pulse voltammetry; DSC, differential scanning calorimetry; T_m/T_c, melting/crystallization temperature; $\Delta H_m/\Delta H_c$, melting/crystallization enthalpy; TEM, electron transmission microscopy; ED, electron diffraction; PTFE, poly(tetrafluoroethylene).

REFERENCES

(1) Koppe, M.; Brabec, C. J.; Heiml, S.; Schausberger, A.; Duffy, W.; Heeney, M.; McCulloch, I. Influence of Molecular Weight Distribution on the Gelation of P3HT and Its Impact on the Photovoltaic Performance. *Macromolecules* **2009**, *42* (13), 4661–4666. https://doi.org/10.1021/ma9005445.

(2) Himmelberger, S.; Vandewal, K.; Fei, Z.; Heeney, M.; Salleo, A. Role of Molecular Weight Distribution on Charge Transport in Semiconducting Polymers. *Macromolecules* **2014**, *47* (20), 7151–7157. https://doi.org/10.1021/ma501508j.

(3) Wang, G.; Melkonyan, F. S.; Facchetti, A.; Marks, T. J. All-Polymer Solar Cells: Recent Progress, Challenges, and Prospects. *Angew. Chem. Int. Ed Engl.* **2019**, *58* (13), 4129–4142. https://doi.org/10.1002/anie.201808976.

(4) Zhu, P.; Fan, B.; Ying, L.; Huang, F.; Cao, Y. Recent Progress in All-Polymer Solar Cells Based on Wide-Bandgap p-Type Polymers. *Chem. – Asian J.* **2019**, *14* (18), 3109–3118. https://doi.org/10.1002/asia.201900827.

(5) Yan, C.; Barlow, S.; Wang, Z.; Yan, H.; Jen, A. K.-Y.; Marder, S. R.; Zhan, X. Non-Fullerene Acceptors for Organic Solar Cells. *Nat. Rev. Mater.* **2018**, *3* (3), 1–19. https://doi.org/10.1038/natrevmats.2018.3.

(6) Wadsworth, A.; Moser, M.; Marks, A.; Little, M. S.; Gasparini, N.; Brabec, C. J.; Baran, D.; McCulloch, I. Critical Review of the Molecular Design Progress in Non-Fullerene Electron Acceptors towards Commercially Viable Organic Solar Cells. *Chem. Soc. Rev.* **2019**, *48* (6), 1596–1625. https://doi.org/10.1039/C7CS00892A.

(7) Sharma, V.; Koenig, J. D. B.; Welch, G. C. Perylene Diimide Based Non-Fullerene Acceptors: Top Performers and an Emerging Class Featuring N-Annulation. *J. Mater. Chem. A* **2021**, *9* (11), 6775–6789. https://doi.org/10.1039/D0TA11197J.

(8) Cui, Y.; Yao, H.; Zhang, J.; Zhang, T.; Wang, Y.; Hong, L.; Xian, K.; Xu, B.; Zhang, S.; Peng, J.; Wei, Z.; Gao, F.; Hou, J. Over 16% Efficiency Organic Photovoltaic Cells Enabled by a Chlorinated Acceptor with Increased Open-Circuit Voltages. *Nat. Commun.* **2019**, *10* (1), 2515. https://doi.org/10.1038/s41467-019-10351-5.

(9) Fan, B.; Zhang, D.; Li, M.; Zhong, W.; Zeng, Z.; Ying, L.; Huang, F.; Cao, Y. Achieving over 16% Efficiency for Single-Junction Organic Solar Cells. *Sci. China Chem.* **2019**, *62* (6), 746–752. https://doi.org/10.1007/s11426-019-9457-5.

(10) Gao, W.; Qi, F.; Peng, Z.; Lin, F. R.; Jiang, K.; Zhong, C.; Kaminsky, W.; Guan, Z.; Lee, C.-S.; Marks, T. J.; Ade, H.; Jen, A. K.-Y. Achieving 19% Power Conversion Efficiency in Planar-Mixed Heterojunction Organic Solar Cells Using a Pseudo-Symmetric Electron Acceptor. *Adv. Mater. n/a* (n/a), 2202089. https://doi.org/10.1002/adma.202202089.

(11) Deshmukh, K. D.; Matsidik, R.; Prasad, S. K. K.; Connal, L. A.; Liu, A. C. Y.; Gann, E.; Thomsen, L.; Hodgkiss, J. M.; Sommer, M.; McNeill, C. R. Tuning the Molecular Weight of the Electron Accepting Polymer in All-Polymer Solar Cells: Impact on Morphology and Charge Generation. *Adv. Funct. Mater.* **2018**, *28* (18), 1707185. https://doi.org/10.1002/adfm.201707185.

(12) Nahid, M. M.; Matsidik, R.; Welford, A.; Gann, E.; Thomsen, L.; Sommer, M.; McNeill, C. R. Unconventional Molecular Weight Dependence of Charge Transport in the High Mobility N-Type Semiconducting Polymer P(NDI2OD-T2). *Adv. Funct. Mater.* **2017**, *27* (9), 1604744. https://doi.org/10.1002/adfm.201604744.

(13) Koch, F. P. V.; Rivnay, J.; Foster, S.; Müller, C.; Downing, J. M.; Buchaca-Domingo, E.; Westacott, P.; Yu, L.; Yuan, M.; Baklar, M.; Fei, Z.; Luscombe, C.; McLachlan, M. A.; Heeney, M.; Rumbles, G.; Silva, C.; Salleo, A.; Nelson, J.; Smith, P.; Stingelin, N. The Impact of Molecular Weight on Microstructure and Charge Transport in Semicrystalline Polymer Semiconductors–Poly(3-Hexylthiophene), a Model Study. *Prog. Polym. Sci.* **2013**, *38* (12), 1978–1989. https://doi.org/10.1016/j.progpolymsci.2013.07.009.

(14) Zhang, P.; Yi, W. H.; Lei, B.; Zhou, J. F.; Tian, Y. L.; Ren, W. Y. Effects of the Molecular Weight of PCz on Selective Extraction of Large-Diameter Semiconducting Single-Walled Carbon Nanotubes. *J. Nano Res.* **2021**, *69*, 11–21. https://doi.org/10.4028/www.scientific.net/JNanoR.69.11.

(15) Wu, Z.; Petzold, A.; Henze, T.; Thurn-Albrecht, T.; Lohwasser, R. H.; Sommer, M.; Thelakkat, M. Temperature and Molecular Weight Dependent Hierarchical Equilibrium Structures in Semiconducting Poly(3-Hexylthiophene). *Macromolecules* **2010**, *43* (10), 4646–4653. https://doi.org/10.1021/ma902566h.

(16) Kim, Y.; Park, H.; Abdilla, A.; Yun, H.; Han, J.; Stein, G. E.; Hawker, C. J.; Kim, B. J. Chain-Length-Dependent Self-Assembly Behaviors of Discrete Conjugated Oligo(3-Hexylthiophene). *Chem. Mater.* **2020**, *32* (8), 3597–3607. https://doi.org/10.1021/acs.chemmater.0c00869.

(17) Ni, Z.; Wang, H.; Dong, H.; Dang, Y.; Zhao, Q.; Zhang, X.; Hu, W. Mesopolymer Synthesis by Ligand-Modulated Direct Arylation Polycondensation towards n-Type and Ambipolar Conjugated Systems. *Nat. Chem.* **2019**, *11* (3), 271–277. https://doi.org/10.1038/s41557-018-0200-y.

(18) Vangerven, T.; Verstappen, P.; Patil, N.; D'Haen, J.; Cardinaletti, I.; Benduhn, J.; Van den Brande, N.; Defour, M.; Lemaur, V.; Beljonne, D.; Lazzaroni, R.; Champagne, B.; Vandewal, K.; Andreasen, J. W.; Adriaensens, P.; Breiby, D. W.; Van Mele, B.; Vanderzande, D.; Maes, W.; Manca, J. Elucidating Batch-to-Batch Variation Caused by Homocoupled Side Products in Solution-Processable Organic Solar Cells. *Chem. Mater.* **2016**, *28* (24), 9088–9098. https://doi.org/10.1021/acs.chemmater.6b04143.

(19) Gundlach, D. J.; Lin, Y.-Y.; Jackson, T. N.; Schlom, D. G. Oligophenyl-Based Organic Thin Film Transistors. *Appl. Phys. Lett.* **1997**, *71* (26), 3853–3855. https://doi.org/10.1063/1.120524.

(20) Linton, K. E.; Fox, M. A.; Pålsson, L.-O.; Bryce, M. R. Oligo(p-Phenyleneethynylene) (OPE) Molecular Wires: Synthesis and Length Dependence of Photoinduced Charge Transfer in OPEs with Triarylamine and Diaryloxadiazole End Groups. *Chem. – Eur. J.* **2015**, *21* (10), 3997–4007. https://doi.org/10.1002/chem.201406080.

(21) Hinderer, F.; May, R.; Jester, S.-S.; Höger, S. Monodisperse Oligo(p-Phenylene–Butadiynylene)s: GPC Conversion Factors and Self-Assembled Monolayers. *Macromolecules* **2016**, *49* (5), 1816–1821. https://doi.org/10.1021/acs.macromol.5b02666.

(22) Zhou, C.-Z.; Liu, T.; Xu, J.-M.; Chen, Z.-K. Synthesis, Characterization, and Physical Properties of Monodisperse Oligo(p-Phenyleneethynylene)s. *Macromolecules* **2003**, *36* (5), 1457–1464. https://doi.org/10.1021/ma021656a.

(23) Xue, C.; Luo, F.-T. Rapid Syntheses of Oligo(p-Phenyleneethynylene)s via Iterative Convergent Approach. *Tetrahedron* **2004**, *60* (30), 6285–6294. https://doi.org/10.1016/j.tet.2004.05.085.

(24) Remmers, M.; Müller, B.; Martin, K.; Räder, H.-J.; Köhler, W. Poly(p-Phenylene)s. Synthesis, Optical Properties, and Quantitative Analysis with HPLC and MALDI–TOF Mass Spectrometry. *Macromolecules* **1999**, *32* (4), 1073–1079. https://doi.org/10.1021/ma981260s.

(25) Mishra, A.; Ma, C.-Q.; Bäuerle, P. Functional Oligothiophenes: Molecular Design for Multidimensional Nanoarchitectures and Their Applications. *Chem. Rev.* **2009**, *109* (3), 1141–1276. https://doi.org/10.1021/cr8004229.

(26) Lawrence, J.; Lee, S.-H.; Abdilla, A.; Nothling, M. D.; Ren, J. M.; Knight, A. S.; Fleischmann, C.; Li, Y.; Abrams, A. S.; Schmidt, B. V. K. J.; Hawker, M. C.; Connal, L. A.; McGrath, A. J.; Clark, P. G.;

Gutekunst, W. R.; Hawker, C. J. A Versatile and Scalable Strategy to Discrete Oligomers. *J. Am. Chem. Soc.* **2016**, *138* (19), 6306–6310. https://doi.org/10.1021/jacs.6b03127.

(27) Koch, F. P. V.; Smith, P.; Heeney, M. "Fibonacci's Route" to Regioregular Oligo(3-Hexylthiophene)s. *J. Am. Chem. Soc.* **2013**, *135* (37), 13695–13698. https://doi.org/10.1021/ja4057932.

(28) Turner, D. J.; Anémian, R.; Mackie, P. R.; Cupertino, D. C.; Yeates, S. G.; Turner, M. L.; Spivey, A. C. Towards a General Solid Phase Approach for the Iterative Synthesis of Conjugated Oligomers Using a Germanium Based Linker - First Solid Phase Synthesis of an Oligo-(Triarylamine). *Org. Biomol. Chem.* **2007**, *5* (11), 1752–1763. https://doi.org/10.1039/B703022C.

(29) Liu, S.-Y.; Cheng, J.-Z.; Zhang, X.-F.; Liu, H.; Shen, Z.-Q.; Wen, H.-R. Single-Step Access to a Series of D–A π-Conjugated Oligomers with 3–10 Nm Chain Lengths. *Polym. Chem.* **2019**, *10* (3), 325–330. https://doi.org/10.1039/C8PY01478G.

(30) Wang, L.-H.; Chen, X.-J.; Ye, D.-N.; Liu, H.; Chen, Y.; Zhong, A.-G.; Li, C.-Z.; Liu, S.-Y. Pot- and Atom-Economic Synthesis of Oligomeric Non-Fullerene Acceptors via C–H Direct Arylation. *Polym. Chem.* **2022**, *13* (16), 2351–2361. https://doi.org/10.1039/D2PY00139J.

(31) Polander, L. E.; Romanov, A. S.; Barlow, S.; Hwang, D. K.; Kippelen, B.; Timofeeva, T. V.; Marder, S. R. Stannyl Derivatives of Naphthalene Diimides and Their Use in Oligomer Synthesis. *Org. Lett.* **2012**, *14* (3), 918–921. https://doi.org/10.1021/ol203432x.

(32) Yan, H.; Chen, Z.; Zheng, Y.; Newman, C.; Quinn, J. R.; Dötz, F.; Kastler, M.; Facchetti, A. A High-Mobility Electron-Transporting Polymer for Printed Transistors. *Nature* **2009**, *457* (7230), 679–686. https://doi.org/10.1038/nature07727.

(33) Guo, X.; Watson, M. D. Conjugated Polymers from Naphthalene Bisimide. *Org. Lett.* **2008**, *10* (23), 5333–5336. https://doi.org/10.1021/ol801918y.

(34) Sommer, M. Conjugated Polymers Based on Naphthalene Diimide for Organic Electronics. *J. Mater. Chem. C* **2014**, *2* (17), 3088–3098. https://doi.org/10.1039/C3TC31755B.

(35) Guo, X.; Facchetti, A.; Marks, T. J. Imide- and Amide-Functionalized Polymer Semiconductors. *Chem. Rev.* **2014**, *114* (18), 8943–9021. https://doi.org/10.1021/cr500225d.

(36) Al Kobaisi, M.; Bhosale, S. V.; Latham, K.; Raynor, A. M.; Bhosale, S. V. Functional Naphthalene Diimides: Synthesis, Properties, and Applications. *Chem. Rev.* **2016**, *116* (19), 11685–11796. https://doi.org/10.1021/acs.chemrev.6b00160.

(37) Takimiya, K.; Nakano, M. Thiophene-Fused Naphthalene Diimides: New Building Blocks for Electron Deficient π-Functional Materials. *Bull. Chem. Soc. Jpn.* **2018**, *91* (1), 121–140. https://doi.org/10.1246/bcsj.20170298.

(38) Insuasty, A.; Maniam, S.; Langford, S. J. Recent Advances in the Core-Annulation of Naphthalene Diimides. *Chem. – Eur. J.* **2019**, *25* (29), 7058–7073. https://doi.org/10.1002/chem.201806009.

(39) Bhosale, S. V.; Kobaisi, M. A.; Jadhav, R. W.; Morajkar, P. P.; Jones, L. A.; George, S. Naphthalene Diimides: Perspectives and Promise. *Chem. Soc. Rev.* **2021**, *50* (17), 9845–9998. https://doi.org/10.1039/D0CS00239A.

(40) Kukhta, N. A.; Marks, A.; Luscombe, C. K. Molecular Design Strategies toward Improvement of Charge Injection and Ionic Conduction in Organic Mixed Ionic–Electronic Conductors for Organic Electrochemical Transistors. *Chem. Rev.* **2022**, *122* (4), 4325–4355. https://doi.org/10.1021/acs.chemrev.1c00266.

(41) Noriega, R.; Rivnay, J.; Vandewal, K.; Koch, F. P. V.; Stingelin, N.; Smith, P.; Toney, M. F.; Salleo, A. A General Relationship between Disorder, Aggregation and Charge Transport in Conjugated Polymers. *Nat. Mater.* **2013**, *12* (11), 1038–1044. https://doi.org/10.1038/nmat3722.

(42) Matsidik, R.; Komber, H.; Luzio, A.; Caironi, M.; Sommer, M. Defect-Free Naphthalene Diimide Bithiophene Copolymers with Controlled Molar Mass and High Performance via Direct Arylation Polycondensation. *J. Am. Chem. Soc.* **2015**, *137* (20), 6705–6711. https://doi.org/10.1021/jacs.5b03355.

(43) Nübling, F.; Komber, H.; Sommer, M. All-Conjugated, All-Crystalline Donor–Acceptor Block Copolymers P3HT-b-PNDIT2 via Direct Arylation Polycondensation. *Macromolecules* **2017**, *50* (5), 1909–1918. https://doi.org/10.1021/acs.macromol.7b00251.

(44) Goto, E.; Ando, S.; Ueda, M.; Higashihara, T. Nonstoichiometric Stille Coupling Polycondensation for Synthesizing Naphthalene-Diimide-Based π-Conjugated Polymers. *ACS Macro Lett.* **2015**, *4* (9), 1004–1007. https://doi.org/10.1021/acsmacrolett.5b00532.

(45) Strawser, D.; Karton, A.; Zenkina, O. V.; Iron, M. A.; Shimon, L. J. W.; Martin, J. M. L.; van der Boom, M. E. Platinum Stilbazoles: Ring-Walking Coupled with Aryl–Halide Bond Activation. *J. Am. Chem. Soc.* **2005**, *127* (26), 9322–9323. https://doi.org/10.1021/ja050613h.

(46) Senkovskyy, V.; Tkachov, R.; Komber, H.; John, A.; Sommer, J.-U.; Kiriy, A. Mechanistic Insight into Catalyst-Transfer Polymerization of Unusual Anion-Radical Naphthalene Diimide Monomers: An Observation of Ni(0) Intermediates. *Macromolecules* **2012**, *45* (19), 7770–7777. https://doi.org/10.1021/ma301797w.

(47) Kiriy, A.; Senkovskyy, V.; Sommer, M. Kumada Catalyst-Transfer Polycondensation: Mechanism, Opportunities, and Challenges. *Macromol. Rapid Commun.* **2011**, *32* (19), 1503–1517. https://doi.org/10.1002/marc.201100316.

(48) Leone, A. K.; McNeil, A. J. Matchmaking in Catalyst-Transfer Polycondensation: Optimizing Catalysts Based on Mechanistic Insight. *Acc. Chem. Res.* **2016**, *49* (12), 2822–2831. https://doi.org/10.1021/acs.accounts.6b00488.

(49) Matsidik, R.; Komber, H.; Sommer, M. Rational Use of Aromatic Solvents for Direct Arylation Polycondensation: C–H Reactivity versus Solvent Quality. *ACS Macro Lett.* **2015**, *4* (12), 1346–1350. https://doi.org/10.1021/acsmacrolett.5b00783.

(50) Matsidik, R.; Luzio, A.; Hameury, S.; Komber, H.; McNeill, C. R.; Caironi, M.; Sommer, M. Effects of PNDIT2 End Groups on Aggregation, Thin Film Structure, Alignment and Electron Transport in Field-Effect Transistors. *J. Mater. Chem. C* **2016**, *4* (43), 10371–10380. https://doi.org/10.1039/C6TC03804B.

(51) Matsidik, R.; Martin, J.; Schmidt, S.; Obermayer, J.; Lombeck, F.; Nübling, F.; Komber, H.; Fazzi, D.; Sommer, M. C–H Arylation of Unsubstituted Furan and Thiophene with Acceptor Bromides: Access to Donor–Acceptor–Donor-Type Building Blocks for Organic Electronics. *J. Org. Chem.* **2015**, *80* (2), 980–987. https://doi.org/10.1021/jo502432e.

(52) Rudenko, A. E.; Thompson, B. C. Influence of the Carboxylic Acid Additive Structure on the Properties of Poly(3-Hexylthiophene) Prepared via Direct Arylation Polymerization (DArP). *Macromolecules* **2015**, *48* (3), 569–575. https://doi.org/10.1021/ma502131k.

(53) Steyrleuthner, R.; Di Pietro, R.; Collins, B. A.; Polzer, F.; Himmelberger, S.; Schubert, M.; Chen, Z.; Zhang, S.; Salleo, A.; Ade, H.; Facchetti, A.; Neher, D. The Role of Regioregularity, Crystallinity, and Chain Orientation on Electron Transport in a High-Mobility n-Type Copolymer. *J. Am. Chem. Soc.* **2014**, *136* (11), 4245–4256. https://doi.org/10.1021/ja4118736.

(54) Sirringhaus, H. 25th Anniversary Article: Organic Field-Effect Transistors: The Path Beyond Amorphous Silicon. *Adv. Mater.* **2014**, *26* (9), 1319–1335. https://doi.org/10.1002/adma.201304346.

(55) Wu, Y.; Schneider, S.; Yuan, Y.; Young, R. M.; Francese, T.; Mansoor, I. F.; Dudenas, P. J.; Lei, Y.; Gomez, E. D.; DeLongchamp, D. M.; Lipke, M. C.; Galli, G.; Wasielewski, M. R.; Asbury, J. B.; Toney, M. F.; Bao, Z. Twisted A-D-A Type Acceptors with Thermally-Activated Delayed Crystallization Behavior for Efficient Nonfullerene Organic Solar Cells. *Adv. Energy Mater. n/a* (n/a), 2103957. https://doi.org/10.1002/aenm.202103957.

(56) Wang, Z.; Gao, K.; Kan, Y.; Zhang, M.; Qiu, C.; Zhu, L.; Zhao, Z.; Peng, X.; Feng, W.; Qian, Z.; Gu, X.; Jen, A. K.-Y.; Tang, B. Z.; Cao, Y.; Zhang, Y.; Liu, F. The Coupling and Competition of Crystallization and Phase Separation, Correlating Thermodynamics and

Kinetics in OPV Morphology and Performances. *Nat. Commun.* **2021**, *12* (1), 332. https://doi.org/10.1038/s41467-020-20515-3.

(57) Gorelsky, S. I. Origins of Regioselectivity of the Palladium-Catalyzed (Aromatic)CH Bond Metalation–Deprotonation. *Coord. Chem. Rev.* **2013**, *257* (1), 153–164. https://doi.org/10.1016/j.ccr.2012.06.016.

(58) Blaskovits, J. T.; Johnson, P. A.; Leclerc, M. Mechanistic Origin of β-Defect Formation in Thiophene-Based Polymers Prepared by Direct (Hetero)Arylation. *Macromolecules* **2018**, *51* (20), 8100–8113. https://doi.org/10.1021/acs.macromol.8b01142.

(59) Adamczak, D.; Passarella, B.; Komber, H.; Becker-Koch, D.; Dolynchuk, O.; Schmidt, S. B.; Vaynzof, Y.; Caironi, M.; Sommer, M. Temperature-Dependent Morphology-Electron Mobility Correlations of Naphthalene Diimide-Indacenodithiophene Copolymers Prepared via Direct Arylation Polymerization. *Mater. Adv.* **2021**, *2* (24), 7881–7890. https://doi.org/10.1039/D1MA00633A.

(60) Yanai, T.; Tew, D. P.; Handy, N. C. A New Hybrid Exchange–Correlation Functional Using the Coulomb-Attenuating Method (CAM-B3LYP). *Chem. Phys. Lett.* **2004**, *393* (1), 51–57. https://doi.org/10.1016/j.cplett.2004.06.011.

(61) McLean, A. D.; Chandler, G. S. Contracted Gaussian Basis Sets for Molecular Calculations. I. Second Row Atoms, Z=11–18. *J. Chem. Phys.* **1980**, *72* (10), 5639–5648. https://doi.org/10.1063/1.438980.

(62) Krishnan, R.; Binkley, J. S.; Seeger, R.; Pople, J. A. Self-consistent Molecular Orbital Methods. XX. A Basis Set for Correlated Wave Functions. *J. Chem. Phys.* **1980**, *72* (1), 650–654. https://doi.org/10.1063/1.438955.

(63) Fazzi, D.; Caironi, M.; Castiglioni., C. Quantum-Chemical Insights into the Prediction of Charge Transport Parameters for a Naphthalenetetracarboxydiimide-Based Copolymer with Enhanced Electron Mobility. *J. Am. Chem. Soc.* **2011**, *133* (47), 19056–19059. https://doi.org/10.1021/ja208824d.

(64) Scholz, R.; Luschtinetz, R.; Seifert, G.; Jägeler-Hoheisel, T.; Körner, C.; Leo, K.; Rapacioli, M. Quantifying Charge Transfer Energies at Donor–Acceptor Interfaces in Small-Molecule Solar Cells with Constrained DFTB and Spectroscopic Methods. *J. Phys. Condens. Matter* **2013**, *25* (47), 473201. https://doi.org/10.1088/0953-8984/25/47/473201.

(65) Steyrleuthner, R.; Schubert, M.; Howard, I.; Klaumünzer, B.; Schilling, K.; Chen, Z.; Saalfrank, P.; Laquai, F.; Facchetti, A.; Neher, D. Aggregation in a High-Mobility n-Type Low-Bandgap Copolymer with Implications on Semicrystalline Morphology. *J. Am. Chem. Soc.* **2012**, *134* (44), 18303–18317. https://doi.org/10.1021/ja306844f.

(66) Koch, F. P. V.; Smith, P.; Heeney, M. "Fibonacci's Route" to Regioregular Oligo(3-Hexylthiophene)s. *J. Am. Chem. Soc.* **2013**, *135* (37), 13695–13698. https://doi.org/10.1021/ja4057932.

(67) Kohn, P.; Huettner, S.; Steiner, U.; Sommer, M. Fractionated Crystallization of Defect-Free Poly(3-Hexylthiophene). *ACS Macro Lett.* **2012**, *1* (10), 1170–1175. https://doi.org/10.1021/mz3003769.

(68) Brinkmann, M.; Gonthier, E.; Bogen, S.; Tremel, K.; Ludwigs, S.; Hufnagel, M.; Sommer, M. Segregated versus Mixed Interchain Stacking in Highly Oriented Films of Naphthalene Diimide Bithiophene Copolymers. *ACS Nano* **2012**, *6* (11), 10319–10326. https://doi.org/10.1021/nn304213h.

(69) Moulin, J.-F.; Brinkmann, M.; Thierry, A.; Wittmann, J.-C. Oriented Crystalline Films of Tris(8-Hydroxyquinoline) Aluminum(III): Growth of the Alpha Polymorph onto an Ultra-Oriented Poly(Tetrafluoroethylene) Substrate. *Adv. Mater.* **2002**, *14* (6), 436–439. https://doi.org/10.1002/1521-4095(20020318)14:6<436::AID-ADMA436>3.0.CO;2-K.

(70) Dorset, D. L. *Structural Electron Crystallography*; Springer Science & Business Media, 1995.

(71) Gaussian 16, Revision C.01, Frisch, M. J.; Trucks, G. W.; Schlegel, H. B.; Scuseria, G. E.; Robb, M. A.; Cheeseman, J. R.; Scalmani, G.; Barone, V.; Petersson, G. A.; Nakatsuji, H.; Li, X.; Caricato, M.; Marenich, A. V.; Bloino, J.; Janesko, B. G.; Gomperts, R.; Mennucci, B.; Hratchian, H. P.; Ortiz, J. V.; Izmaylov, A. F.; Sonnenberg, J. L.; Williams-Young, D.; Ding, F.; Lipparini, F.; Egidi, F.; Goings, J.; Peng, B.; Petrone, A.; Henderson, T.; Ranasinghe, D.; Zakrzewski, V. G.; Gao, J.; Rega, N.; Zheng, G.; Liang, W.; Hada, M.; Ehara, M.; Toyota, K.; Fukuda, R.; Hasegawa, J.; Ishida, M.; Nakajima, T.; Honda, Y.; Kitao, O.; Nakai, H.; Vreven, T.; Throssell, K.; Montgomery, J. A., Jr.; Peralta, J. E.; Ogliaro, F.; Bearpark, M. J.; Heyd, J. J.; Brothers, E. N.; Kudin, K. N.; Staroverov, V. N.; Keith, T. A.; Kobayashi, R.; Normand, J.; Raghavachari, K.; Rendell, A. P.; Burant, J. C.; Iyengar, S. S.; Tomasi, J.; Cossi, M.; Millam, J. M.; Klene, M.; Adamo, C.; Cammi, R.; Ochterski, J. W.; Martin, R. L.; Morokuma, K.; Farkas, O.; Foresman, J. B.; Fox, D. J. Gaussian, 2016.

(72) Autschbach, J.; Srebro, M. Delocalization Error and "Functional Tuning" in Kohn–Sham Calculations of Molecular Properties. *Acc. Chem. Res.* **2014**, *47* (8), 2592–2602. https://doi.org/10.1021/ar500171t.

(73) Tomasi, J.; Mennucci, B.; Cammi, R. Quantum Mechanical Continuum Solvation Models. *Chem. Rev.* **2005**, *105* (8), 2999–3094. https://doi.org/10.1021/cr9904009.

(74) Grimme, S.; Ehrlich, S.; Goerigk, L. Effect of the Damping Function in Dispersion Corrected Density Functional Theory. *J. Comput. Chem.* **2011**, *32* (7), 1456–1465. https://doi.org/10.1002/jcc.21759.

(75) Wang, X.; Zhang, F.; Schellhammer, K. S.; Machata, P.; Ortmann, F.; Cuniberti, G.; Fu, Y.; Hunger, J.; Tang, R.; Popov, A. A.; Berger, R.; Müllen, K.; Feng, X. Synthesis of NBN-Type Zigzag-Edged Polycyclic Aromatic Hydrocarbons: 1,9-Diaza-9a-Boraphenalene as a Structural Motif. *J. Am. Chem. Soc.* **2016**, *138* (36), 11606–11615. https://doi.org/10.1021/jacs.6b04445.

(76) Brinkmann, M.; Graff, S.; Straupé, C.; Wittmann, J.-C.; Chaumont, C.; Nuesch, F.; Aziz, A.; Schaer, M.; Zuppiroli, L. Orienting Tetracene and Pentacene Thin Films onto Friction-Transferred Poly(Tetrafluoroethylene) Substrate. *J. Phys. Chem. B* **2003**, *107* (38), 10531–10539. https://doi.org/10.1021/jp030217q.

TOC Figure

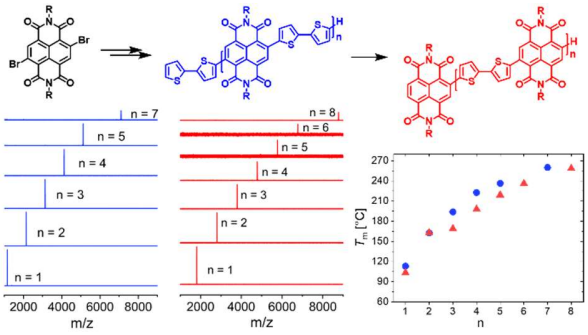
n = 7
n = 5
n = 4
n = 3
n = 2
n = 1
2000 4000 6000 8000
m/z
n = 8
n = 6
n = 5
n = 4
n = 3
n = 2
n = 1
2000 4000 6000 8000
m/z
270
240
210
180
150
120
90
60
T_m [°C]
1 2 3 4 5 6 7 8
n